



ISSN: 0067-2904

Properties of Ground-State of $^{17,19,20,24,26}\text{F}$ using the Wave Functions of Harmonic-Oscillator and Spherical Hankel Functions

Saif Ali J. Khalaf*, Arkan R. Ridha

Department of Physics, College of Science, University of Baghdad, Baghdad-Iraq

Received: 28/3/2022

Accepted: 1/8/2022

Published: 28/2/2023

Abstract

The nuclear size radii, density distributions and elastic electron scattering charge form factors for Fluorine isotopes ($^{17,19,20,24,26}\text{F}$) were studied using the radial wave functions (WF) of harmonic-oscillator (HO) potential and free mean field described by spherical Hankel functions (SHF) for the core and the valence parts, respectively for all aforementioned isotopes. The parameters for HO potential (size parameter b) and SHF were chosen to regenerate the available experimental size radii. It was found that using spherical Hankel functions in our work improved the calculated results quantities in comparison with empirical data.

Keywords: Halo nuclei, size radii, density distributions, electron scattering charge form factors, shell model, proton-rich nuclei and neutron-rich nuclei

PACS Nos: 21.10.ft, 21.10.Gv, 21.60.Cs, 25.30.Bf

خصائص الحالة الارضية لنظائر الفلور $^{17,19,20,24,26}\text{F}$ باستخدام الدوال الموجية للمتنذبذ التوافقي ودوال هانكل الكروية

سيف علي جعفر خلف* ، اركان رفعة رضا

قسم الفيزياء، كلية العلوم، جامعه بغداد، بغداد، العراق

الخلاصة

تم دراسة أنصاف الأقطار النووية وتوزيعات الكثافة وعوامل التشكل الشحنة للاستطارة الألكترونية المرنة لنظائر الفلور ($^{17,19,20,24,26}\text{F}$) باستخدام الدوال الموجية الشعاعية للمتنذبذ التوافقي المستخدمة لدراسة اجزاء القلب بينما اجزاء التكافؤ لنفس النظائر تمت دراستها باستخدام دوال هانكل الكروية. معلمات الدوال الموجية للمتنذبذ التوافقي و دوال هانكل الكروية ثبتت واختيرت بحيث تولد انصاف الاقطار العملية لجميع نظائر الفلور قيد الدراسة. وجدنا في عملنا الحالي ان ادخال الدوال الموجية لهانكل الكروية ادت الى تحسين النتائج للكميات المحسوبة مقارنة مع الداتا العملية.

1. Introduction

Tanihita's discovery of an exotic nucleus four decades ago sparked tremendous experimental and theoretical studies. The unusual ratio of protons to neutrons or vice versa leads to exoticism in the ground and excited state structures of these nuclei [1]. One of the

*Email: done.dd9000@gmail.com

unusual structures of such nuclei is the long tail in density distribution and extraordinary size radii. Such phenomenon is called the halo [2]. Besides, the energy of the last proton or neutron in the final orbit is less than 1 MeV and prefers to be in orbits with angular momentum $l = 0$ or $l = 1$ [3]. In contrast to stable nuclei, one should imply theoretical changes in the nuclear models to study the properties of exotic nuclei [4]. In theoretical calculations, the wave function is the key tool for studying the bulk properties of nuclei. The HO WFs can be used but with limitations; their asymptotic behavior at large r is described by Gaussian fall behavior [5,6]. As a result, changes must be made; HO WFs with two HO size parameters have been used with acceptable results for some exotic nuclei [7,8]. The transformed HO basis obtained by Local Scale Transformation (LST) is a promising method for regenerating the long tail behavior in the density distribution [9,10]. The single-particle wave functions of the HO and Woods-Saxon (WS) potential are employed to investigate the stable core and unstable halo parts [11,12].

An advantage of our present study is the use of Spherical Hankel Functions (SHF) to investigate the tail part of stable and exotic isotopes of Fluorine ($^{17,19,20,24,26}\text{F}$). The size radii, density distributions, charge form factors were also studied. The SHF are used to describe the valence orbits, whereas the HO WFs are used to describe the core.

2. Theoretical Bases

for free mean field, $U(r) = 0$ and $E_{l,t_z} = -\varepsilon_{l,t_z}$ (where E_{nlj,t_z} stands for the binding energy of the last nucleons(s)), the radial part of Schrodinger equation can be written as[13]:

$$\left[\frac{d^2}{dr^2} + \frac{2}{r} \frac{d}{dr} - \frac{2\mu}{\hbar^2} \left(\varepsilon_{l,t_z} + \frac{l(l+1)}{2\mu r^2} \right) \right] k_{l,t_z}(r) = 0 \quad (1)$$

Where: $k_{l,t_z}(r)$ stands for the solution to Eq. (1), n, l, j and t_z are the principle quantum number, the orbital quantum number, total spin quantum number of a single particle and the projection of isospin quantum number of a single particle ($t_z = \frac{1}{2}$ for proton and $t_z = -\frac{1}{2}$ for neutron), respectively. It is clear that Eq. (1) describes the modified Bessel differential equation which has two solutions; the modified Bessel functions of the first and second ranks. The impotent solution is of the second rank at the region $r > R_c$ (R_c is the point where the wave function of the core and the MBF intersect) is given in terms of spherical Hankel functions (SHF) of the first kind [14,15]

$$k_{l,t_z}(r) = -i^l h_{l,t_z}^{(1)}(ir) \quad (2)$$

since,

$$h_{l,t_z}^{(1)}(r) = (-i)^{l+1} \frac{e^{i\chi_{l,t_z} r}}{\chi_{l,t_z} r} \sum_{m=0}^l \frac{(l+m)(i)^m}{m!(l-m)!(2r)^m} \quad (3)$$

The χ_{l,t_z} ($\chi_{l,t_z} = \sqrt{\frac{2\mu\varepsilon_{l,t_z}}{\hbar}}$) and μ denote the attenuation parameter and the reduced mass among the core-valence system), respectively. Eq. (3) can be written in terms of Whittaker's functions [14]:

$$k_{l,t_z}(r) = \frac{w_{0,l+\frac{1}{2}}(2\chi_{l,t_z} r)}{\chi_{l,t_z} r} \quad (4)$$

where

$$w_{0,l+\frac{1}{2}}(2\chi_{l,t_z}r) = e^{-i\chi_{l,t_z}r} \sum_{k=0}^l \frac{(l+k)!}{2^k k! (l-k)! (\chi_{l,t_z}r)^k} \tag{5}$$

For HO potential, $U(r) = -V_0 + \frac{1}{2}m_{t_z}\omega^2r^2$, Eq. (1) has the solution [16]:

$$R_{nl}(r, b_{t_z}) = \frac{1}{(2l+1)!!} \left[\frac{2^{l-n+3}(2n+2l-1)!!}{\sqrt{\pi}b_{t_z}^3(n-1)!} \right]^{\frac{1}{2}} \left(\frac{r}{b_{t_z}} \right)^l e^{-\frac{r^2}{2b_{t_z}^2}} \sum_{k=0}^{n-1} (-1)^k \frac{(n-1)!2^k(2l+1)!!}{(n-k-1)!k!(2l+2k+1)} \left(\frac{r}{b_{t_z}} \right)^{2k} \tag{6}$$

In Eq. (6), b_{t_z} represents the HO size parameter for neutrons or protons.

The proton and neutron density distributions for stable ^{19}F nuclide is calculated from:

$$\rho_{t_z}(r) = \frac{1}{4\pi} \sum_{a \in \text{core}} n_{a,t_z} |R_{n_a l_a}(r, b_{t_z})|^2 + \frac{A_{l,t_z}}{4\pi} n_{l,t_z} |k_l(\chi_{l,t_z}r)|^2 \tag{7}$$

Where A_{l,t_z} represents the amplitude of the valence part (determined from normalization the of neutron and proton numbers).

The proton and neutron density distributions for neutron rich isotopes can be written, respectively as:

$$\rho_{t_z=p}(r) = \frac{1}{4\pi} \sum_{a \in \text{core}} n_{a,t_z=p} |R_{n_a l_a}(r, b_{t_z=p})|^2 \tag{8}$$

$$\rho_{t_z=n}(r) = \frac{1}{4\pi} \sum_{a \in \text{core}} n_{a,t_z=n} |R_{n_a l_a}(r, b_{t_z=n})|^2 + \frac{A_{l,t_z=n}}{4\pi} n_l |k_l(\chi_{l,t_z=n}r)|^2 \tag{9}$$

Where n_{a,t_z} represents the number of protons(neutrons) in the shell a within the core (a denotes the quantum numbers, n and l). The n_l stands for the number of neutron(s) in the valence part.

From Eqs. (7), (8) and (9), the charge density distribution (CDD) is computed as [10]:

$$\rho_{ch}(r) = \rho_{ch,t_z=p}(r) + \rho_{ch,t_z=n}(r) \tag{10}$$

where

$$\rho_{ch,t_z=p}(r) = \int \rho_{t_z=p}(r) \rho_{pr}(\mathbf{r} - \mathbf{r}') d\mathbf{r}' \tag{11}$$

and

$$\rho_{ch,t_z=n}(r) = \int \rho_{J=0,t_z=n}(r) \rho_{neu}(\mathbf{r} - \mathbf{r}') d\mathbf{r}' \tag{12}$$

$\rho_{pr}(\vec{r})$ and $\rho_{neu}(\vec{r})$ in Eq.(11) and Eq.(12) represent the CDDs of the single proton and neutron, as defined by Elton [17] and Chandra and Sauer[18].

The root mean square (*rms*) of proton, neutron, charge and matter radii are calculated from the following equation [18]:

$$\langle r^2 \rangle_x^{1/2} = \sqrt{\frac{4\pi}{x} \int_0^\infty \rho_x(r) r^4 dr} \tag{13}$$

x stands for the proton, neutron, charge and matter.

Finally, the electron scattering Coulomb form factors in the plane-wave Born approximation for J multipole can be written as:

$$F_{ch}^J(q) = \frac{4\pi}{z} \int_0^\infty j_J(qr) \rho_{ch}^J(r) r^2 dr \tag{14}$$

3. Results and discussion

The nuclear shell model with HO WFs and SHFs was used to determine the *rms* radii, density distributions, and charge form factors for the isotopes ^{17,20,24,26}F. The core parts for all isotopes under study were investigated using HO WFs, whereas SHF were used for valence parts. Such treatment, denoted by HO+SHF, were represented in the computations, knowing that ¹⁹F is stable isotope while ^{17,20,24,26}F are exotic ones.

In Table 1, the total spin and parity (*J^π*), the total isospin (*T*), the half-life time (*t*_{1/2}), the HO size parameters (*b_c*) for protons and neutrons in the core, the *χ_{l,tz}* and single –nucleon separation energies for the last proton (*ε_p*) and neutron (*ε_n*) are shown for ^{17,19,20,24,26}F.

Table 1: the *J^π* *T*, the (*t*_{1/2}), the and single-nucleon binding energies for Fluorine isotope

^A ZX _N (<i>J^π</i> <i>T</i>) [19]	<i>t</i> _{1/2} (s) [19]	<i>b_{c,n}</i> and <i>b_{c,p}</i> (fm)	<i>χ_n</i> and <i>χ_p</i> (fm ⁻¹)	Exp. <i>ε_n</i> (MeV)[20]	Exp. <i>ε_p</i> (MeV)[20]
¹⁷ ₉ F ₈ ($\frac{5^+}{2} \frac{1^-}{2}$)	64.37 ± 0.027s	<i>b_{c,n}</i> =1.652 <i>b_{c,p}</i> = 1.7	<i>χ_{0,p}</i> = 0.165	16.7947986 ± 0.0053699	0.6002676 ± 0.0002479
¹⁹ ₉ F ₁₀ ($\frac{5^+}{2} \frac{1^+}{2}$)	stable	<i>b_{c,n}</i> =1.8 <i>b_{c,p}</i> =1.77	<i>χ_{0,p}</i> = 0.488 <i>χ_{0,n}</i> = 0.970	10.4318757 ± 0.0004633	7.9935998 ± 0.000001
²⁰ ₉ F ₁₁ (0 ⁺ 2 ⁺)	11 ± 0.008 s	<i>b_{c,n}</i> =1.8 <i>b_{c,p}</i> =1.67	<i>χ_{1,n}</i> = 0.550	6.6013362 ± 0.0000297	10.6392921 ± 0.0026371
²⁴ ₉ F ₁₅ (0 ⁺ 3 ⁺)	384 ± 0.016 ms	<i>b_{c,n}</i> =1.7 <i>b_{c,p}</i> =1.58	<i>χ_{0,n}</i> = 0.419	3.8120656 ± 0.1031976	14.3658258 ± 0.1560553
²⁶ ₉ F ₁₇ (1 ⁺ 4 ⁺)	8.2 ± 0.0009 ms	<i>b_{c,n}</i> = 2 <i>b_{c,p}</i> =1.9	<i>χ_{1,n}</i> = 0.184	0.7308299 ± 0.1448941	15.9433462 ± 0.1967426

In Table 2, the computed size radii for ^{17,19,20,24,26}F are tabulated and compared with the experimental values. The parameters presented in Table 1 were chosen to gain as high a match as possible for the calculated size radii in comparison with the experimental data for Fluorine isotopes.

Table 2: Calculated and experimental charge, rms proton, neutron, matter radii for ^{17,19,20,24,26}F

^A ZX _N	Calculated $\langle r^2 \rangle_{ch}^{1/2}$	Exp. $\langle r^2 \rangle_{ch}^{1/2}$	Calculated $\langle r^2 \rangle_p^{1/2}$	Exp. $\langle r^2 \rangle_p^{1/2}$	Calculated $\langle r^2 \rangle_n^{1/2}$	Exp. $\langle r^2 \rangle_n^{1/2}$	Calculated $\langle r^2 \rangle_m^{1/2}$	Exp. $\langle r^2 \rangle_m^{1/2}$
¹⁷ F	2.985	-	2.913	2.90 ± 0.015[21]	2.437	2.478 ± 0.18[21]	2.70	2.71 ± 0.18[21]
¹⁹ F	2.90	-	2.810	-	2.698	2.55 ± 0.15[23]	2.752	2.75 ± 0.07[22]
²⁰ F	2.674	-	2.580	-	2.912	2.90 ± 0.06[23]	2.768	2.79 ± 0.03[22]
²⁴ F	2.531	-	2.441	-	3.308	3.29 ± 0.09[23]	3.012	3.03 ± 0.06[22]
²⁶ F	3.006	-	2.936	-	3.477	3.53 ± 0.17[23]	3.300	3.23 ± 0.13[22]

In Figure 1(a) the calculated CDD and in (b) the charge form factors for ^{19}F are portrayed for ^{19}F . In Figure 1(a), the computed CDD agrees very good with the experimental data [25]. In Figure 1 (b), the determined charge form factor agreed well in comparison with empirical data of Brown et al. [24].

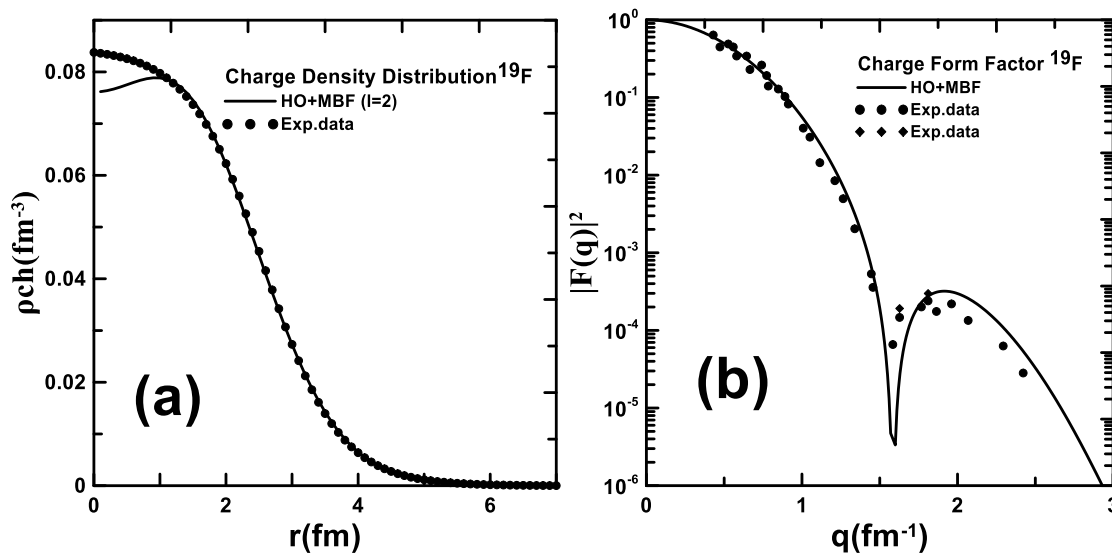
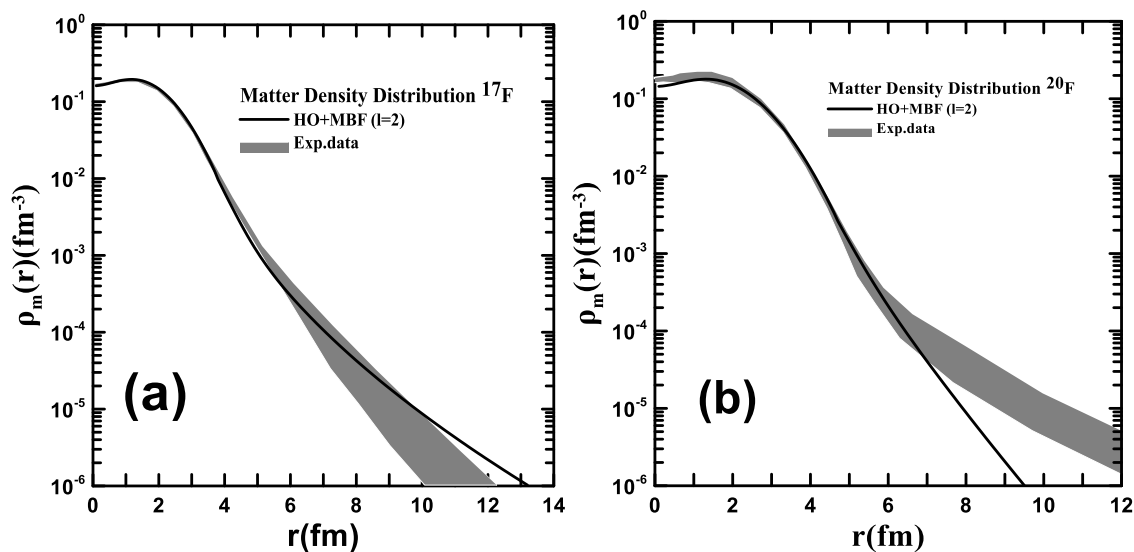


Figure 1: The computed CDD and charge form factor for ^{19}F . Solid curves represent theoretical results. The experimental data for CDD in (a) are denoted by dotted line [25]. The dotted and rhombic lines in (b) represent the experimental charge form factor taken Brown et al. [24].

In Figure (2): (a), (b), (c), and (d) the computed MDDs for $^{17,20,24,26}\text{F}$ are illustrated by solid curves, respectively, the experimental data are shown by shaded areas. In Figures 2 (a) and (d) for $^{17,26}\text{F}$, the computed results are in very good agreement with empirical data, where the long tail are well produced. For ^{20}F and ^{24}F , since their binding energies are very high (see Table 1), the tall pushed highly towards the core, as can be seen in Figure 2(b) and (c). In general, the results are in good agreement with the empirical data. Through the figure and Table 1, it was found that $^{17,26}\text{F}$ with one-proton and one-neutron is a halo isotope, while $^{20,24}\text{F}$ is a neutron isotope of the skin.



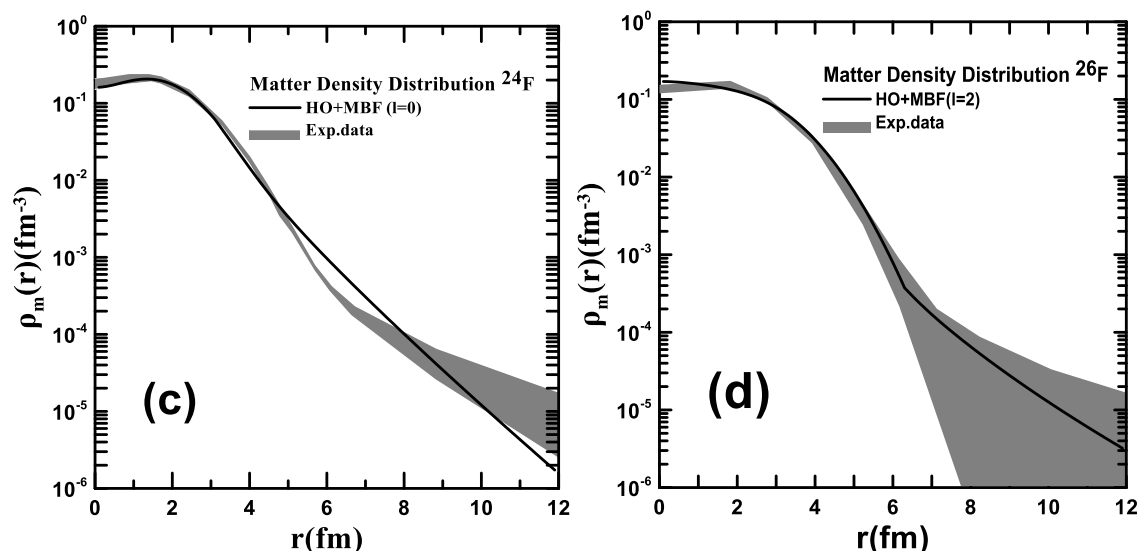


Figure 2: The MDDs computed for ^{17}F , ^{20}F , ^{24}F , and ^{26}F (solid curves). The shaded areas (in a) represent the experimental data (from. Zhang et al. [21]), the shaded areas of (b), (c) and (d) are from Ozawa et al. [22].

In Figure 3(a) and (b), the calculated MDDs and charge form factors for $^{17,19,20,24,26}\text{F}$ are displayed together for comparison. The calculated are symbolized by solid, short-dashed, long-dashed, medium-dashed and dashed-dotted curves for $^{17,19,20,24,26}\text{F}$, respectively. In Figure 3(a), it is clear that with increasing neutron numbers, the single-neutron binding energy decreases, consequently, the long tail in the calculated MDDs increases; leading to the upward shift due to the increase in the tunneling effect. In Figure 3(b), it is obvious that with increasing neutron numbers, the calculated charge form factors shifted backwards and downwards.

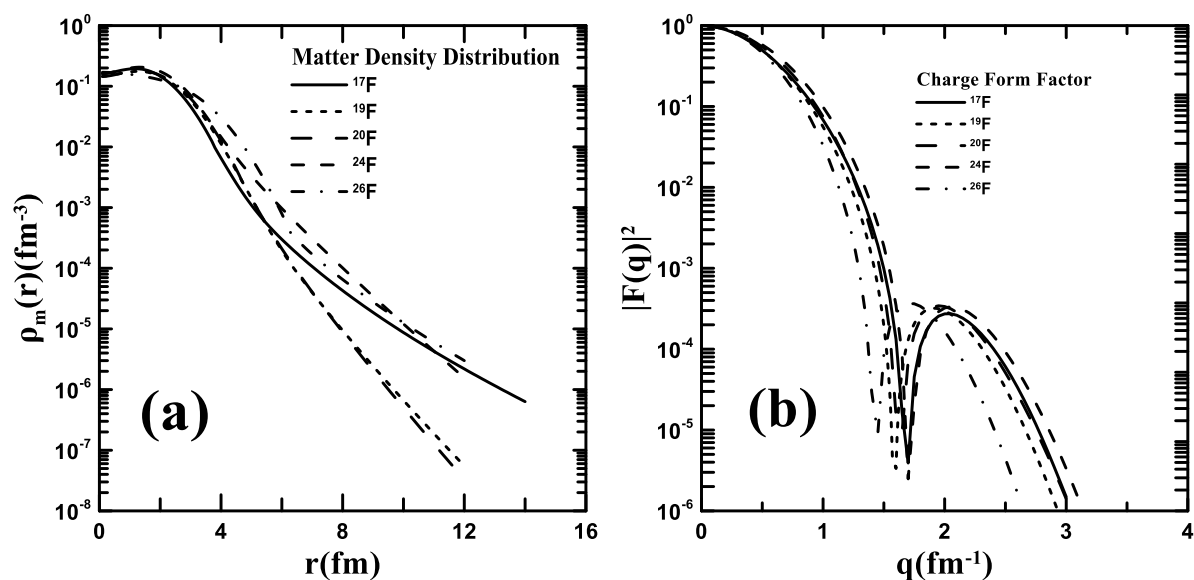


Figure 3: (a) The computed MDDs (b) The charge form factors for $^{17,19,20,24,26}\text{F}$.

4. Conclusions

In conclusion, the ground state properties (size radii, density distributions and charge structure factors) of Fluorine isotopes ($^{17,19,20,24,26}\text{F}$) were investigated. The Spherical Hankel Functions (SHF) are harnessed to study the valence part of all isotopes under study. The core

parts are investigated using the HO WFs. The parameters of HO WFs and SHF were adjusted to regenerate the available experimental *rms* proton, neutron, charge and matter radii. For stable ^{19}F , it was found that there was a very agreement with the experimental data for the computed CDD and charge form factors. For exotic $^{17,26}\text{F}$, a very agreement was found for the computed MDDs with the empirical data. While, for exotic $^{20,24}\text{F}$, an underestimation in the calculated MDDs in comparison with the empirical data was found due to the high binding energies for the last neutron in valence parts leading to pushing the tail part of the MDDs inwards. Besides, it is worth noting that with the decrease of the binding energy of the valence neutron, the tail in the computed MDDs shifted upwards; this is attributed to the increased tunneling effect.

5. References

- [1] I. Tanihata, H. Savajols, R. Kanungo, "Recent experimental progress in nuclear halo structure studies," *Progress in Particle and Nuclear Physics*, vol. 68, pp. 215-313, 2013.
- [2] P. G. Hansen and B. Jonson, "The neutron halo of extremely neutron-rich nuclei," *EPL (Europhysics Letters)*, vol. 4, no. 4, P. 409, 1987.
- [3] I. Tanihata, "Neutron halo nuclei," *Journal of Physics G: Nuclear and Particle Physics*, vol. 22, no. 2, p. 157, 1996.
- [4] A. Covello, editor. *Nuclear Structure Far from Stability: New Physics and New Technology*, vol. 169. IOS Press, 2008.
- [5] W. Nörtershäuser, A. Dax, G. Ewald, S. Götze, R. Kirchner, H.-Jürgen Kluge, T. Kühl, R. Sanchez, A. Wojtaszek, B. A. Bushaw, G. W. F. Drake, Zong-Chao Yan and C. Zimmermann, "First Measurement of the Nuclear Charge Radii of Short-Lived Lithium Isotopes," *In Laser 2004*. Springer, Berlin, Heidelberg, vol. 162, pp. 93–100, 2006.
- [6] M. Brodeur, T. Brunner, S. Effenauer, A.T. Gallant, V. V. Simon, M. Smith, A. Lapierre, E. Mané, R. Ringle, V. L. Ryjkov and S. Bacca, p. Delheij, D. Lunney, M. Pearson, and J. Dilling, "Precision mass measurements of neutron halo nuclei using the TITAN Penning trap," *Hyperfine Interactions*, vol. 199, no. 1, pp.167-173, 2011.
- [7] A. K. Hamoudi, A. R. Radhi, A. R. Ridha, "Theoretical study of matter density distribution and elastic electron scattering form factors for the neutron-rich ^{22}C exotic nucleus," *Iraqi Journal of Physics*, vol. 10, no. 19, pp. 25-34, 2012.
- [8] A. R. Radhi, A. K. Hamoudi and A. R. Ridha R, "Elastic Electron Scattering from Unstable Neutron-Rich ^{19}C Exotic Nucleus," *Iraqi Journal of science*, vol. 54, no. 2, pp. 324-332, 2013.
- [9] M. K. Suhayeb and A. R. Ridha, "Theoretical study of nuclear density distributions and elastic electron scattering form factors for some halo nuclei," *Journal of Science*, vol. 58, no.4B, pp: 2098-2106, 2017.
- [10] S. H. Mohammed, and A. R. Ridha, "Theoretical Study of the Electromagnetic Structure of Boron Isotopes Using Local Scale Transformation Technique," *Iraqi Journal of Science*, vol. 59, no. 4A, pp. 1866-1877, 2018.
- [11] R. I. Noori and A. R. Ridha, "Density Distributions and Elastic Electron Scattering Form Factors of Proton-rich ^8B , ^{17}F , ^{17}Ne , ^{23}Al and ^{27}P Nuclei," *Iraqi Journal of Science*, vol. 60, no. 6, pp. 1286-1296, 2019.
- [12] A. R. Ridha and W. Z. Majeed, "Theoretical Study of Elastic Electron Scattering from ^8B , ^{17}Ne , ^{11}Be and ^{11}Li Halo Nuclei," *Iraqi Journal of Science*, vol. 63, no. 3, pp: 977-987, 2022.
- [13] K. G. Heyde, "The Nuclear Shell Model", Springer – Verlag, Berlin, Heidelberg, 1994.
- [14] F. W. Olver, D. W. Lozier, R. F. Boisvert, C. W. Clark, editors. *NIST handbook of mathematical functions hardback and CD-ROM*. Cambridge university press; 2010.
- [15] J. B. Marion, M. A. Heald, "Classical Electromagnetic Radiation," Academic Press, 1980.
- [16] P. J. Brussard and P. W. M. Glaudemans; "Shell-Model Application in Nuclear spectroscopy", North-Holland, Amsterdam 1977 and R. D. Lawson, "Theory of the nuclear shell model", Clarendon press. Oxford 1980.
- [17] L. R. B. Elton, "Nuclear Sizes", Oxford University Press 1961.
- [18] H. Chandra and G. Sauer, "Relativistic corrections to the elastic electron scattering from ^{208}Pb ," *Phys. Rev C*, vol. 13, no.1, pp. 245-252, 1975.

- [19] F.G Kondev, M. Wang, W.J Huang, S. Naimi, G. Audi, "The NUBASE2020 evaluation of nuclear physics properties," *Chinese Physics C*, vol. 45, no. 3, pp. 030001 2021.
- [20] M. Wang, G. Audi, F. G. Kondev, W.J. Huang, S. Naimi, and X. Xu, "The AME2016 atomic mass evaluation (II). Tables, graphs and references," *Chinese Physics C*, vol. 41, no. 3, pp. 030003, 2017.
- [21] H. Y. Zhang, W. Q. Shen, Z. Z. Ren, Y. G. Ma, W. Z. Jiang, Z. Y. Zhu, Z. Q. Chen, X.Z. Cai, D.Q.Fang, C. Zhong, L. P. Yu, Y. B. Wei, W.L. Zhan, Z.Y. Guo, G.Q. Xiao, J.S. Wang, J.C. Wang, Q.J. Wang, J.X. Li, M. Wang, Z.Q. Chen, "Measurement of reaction cross section for proton-rich nuclei ($A < 30$) at intermediate energies," *Nuclear Physics A*, vol. 707, no. 3-4, pp. 303-324, 2002.
- [22] A. Ozawa, T. Suzuki, I. Tanihata, "Nuclear size and related topics," *Nuclear Physics A*, vol. 693, no. 1-2, pp. 32-62, 2001.
- [23] S. Ahmad, A. A. Usmani, Z. A. Khan, "Matter radii of light proton-rich and neutron-rich nuclear Isotopes," *Physical Review C*, vol. 96, no. 6, pp. 064602, 2017.
- [24] B. A. Brown, B. H. Wildenthal, C. F. Williamson, F. N. Rad, S. Kowalski, H. Crannell and J. T. O'Brien, "Shell-model analysis of high-resolution data for elastic and inelastic electron scattering on ^{19}F ," *Physical Review C: Nucl Phys.*, vol. 32, no. 4, pp. 1127, 1985.
- [25] H. De Vries, C. W. De Jager, and C. De Vries, "Nuclear charge-density- distribution parameters from elastic electron scattering," *Atomic data and nuclear data tables*, vol. 36, no. 3, pp. 495-536, 1987.